RMetS
Royal Meteorological Society

Rainfall along the coast of Peru during strong El Niño events

Janeet Sanabria,[a,b]* Luc Bourrel,[a] Boris Dewitte,[c,d,e] Frédéric Frappart,[a,c] Pedro Rau,[a] Olimpio Solis[b] and David Labat[a]

[a] *UMR 5563 GET, Université de Toulouse - CNRS - IRD - OMP - CNES, France*
[b] *SENAMHI, Lima, Peru*
[c] *UMR 5566 LEGOS, Université de Toulouse - CNRS - IRD - OMP - CNES, France*
[d] *Centro de Estudios Avanzado en Zonas Áridas, Coquimbo, Chile*
[e] *Departamento de Biología, Facultad de Ciencias del Mar, Universidad Católica del Norte, Coquimbo, Chile*

ABSTRACT: While, climatologically, most areas of the Peruvian Pacific region do not experience precipitation, they can be affected by heavy rain and flooding during strong El Niño events with severe socio-economic impacts. Only four strong El Niño events took place within the last five decades (1972/1973, 1982/1983, 1997/1998 and 2015/2016) which led to significant rainfall events in the northern part of Peru. Here a detailed analysis of the evolution of precipitation during these events was performed using gauge records from 1964 to 2016 from a network of 145 meteorological stations located along the Peruvian Pacific region. Through empirical orthogonal function analysis, the rainfall anomalies variability is interpreted as resulting from the combination of a meridional see-saw mode (North–South) (Ep mode) and a zonal see-saw mode (East–West) (Cp mode) that represent, respectively, 34 and 21% of the explained variance. It is shown that the extreme 1982/1983 and 1997/1998 El Niño events have a dominant projection on the Ep mode that has a strong loading in the northern region, while the 1972/1973 and 2015/2016 El Niño events have a relatively weak projection onto the Ep mode (about ten times less at the peak rainy season than the extreme events) and mostly project onto the Cp mode. Also, it is shown that while all events are associated with positive rainfall anomalies in the northern part of Peru which is accounted for by the Ep mode, the evolution of rainfall anomalies along the Cp mode exhibits a significant dispersion. This suggests that the impact of strong El Niño events on the highlands along the coast cannot solely be inferred from the magnitude of the sea surface temperature anomalies in the central equatorial Pacific. Overall, our study illustrates the nonlinearity of the ENSO teleconnection on the rainfall along the coast of Peru during strong El Niño events.

KEY WORDS   strong El Niño events; rainfall anomalies variability; rainfall anomalies modes; rainfall; Peruvian Pacific coast; highlands

Received 24 January 2017; Revised 5 July 2017; Accepted 18 August 2017

1. Introduction

The El Niño Southern Oscillation (ENSO) is the largest mode of climate variability at the interannual time scale. It has a strong impact on many regions surrounding the Pacific Ocean. The ENSO phenomenon influences the regional climate remotely through so-called teleconnections. First, ENSO is associated with the release of adiabatic heat to the troposphere, modifying main atmospheric pathways, leading to the so-called atmospheric teleconnections (Bjerknes, 1969; Horel and Wallace, 1981; Keshavamurty, 1982; Philander, 1985; Trenberth *et al.*, 1998; Diaz *et al.*, 2001). The atmospheric ENSO teleconnections have been extensively studied as they can provide a mechanism by which the main mode of interannual variability in the tropics, that is ENSO, can impact regional climate over the globe. For the coast of Peru where dry mean conditions usually prevail south of 7°S, these are

particularly spectacular during strong El Niño events, because the coastal region experiences heavy rainfall as far south as the Lima region (Takahashi and Martinez, 2017). Second, ENSO is associated with planetary oceanic wave activity along the equator (i.e. Kelvin wave) which can propagate along the coasts of South America and alter the local oceanic circulation in regions which usually experience a persistent upwelling (Clarke, 1983). Countries such as Ecuador and Peru are particularly sensitive to this type of teleconnection, known as oceanic teleconnection. Previous studies have shown in particular that when the sea surface temperature (SST) off Païta (5°S) reaches ∼26 °C, episodes of heavy rainfall can take place suggesting formation of deep local convection under coastal warm SST like what happens in the central western Pacific at large scale (e.g. Woodman, 1999).

Northern Peru has previously experienced devastating rainfall events during El Niño events. For instance, the cost on society and economy associated with the 1982/1983 El Niño event has been estimated at US$ 3.283 million while the 1997/1998 El Niño event exceeded US$ 3.500 million; these values equate to 11.6 and 6.2% of the

---

* Correspondence to: J. Sanabria, UMR 5563 GET, Université de Toulouse - CNRS - IRD - OMP - CNES, Toulouse 31400, France. E-mail: janeet.sanabria@get.omp.eu

respective annual gross domestic product (GDP) (Vargas, 2009).

While it is expected that strong El Niño events impact rainfall in the north of Peru, there is still uncertainty on the magnitude and extent of anomalous rainfall patterns during those events (Rau *et al.*, 2017). This is due to the complex of physical processes at work and the limited number of registered strong events (only four since the 1950s) preventing robust statistics. Another limitation is attributed to the diversity of ENSO. Recent studies pointed out that ENSO can be understood as resulting from at least two distinct regimes (Kao and Yu, 2009; Takahashi *et al.*, 2011; Capotondi *et al.*, 2015) which encompass the two different types of events (Yeh *et al.*, 2009; Takahashi *et al.*, 2011). Extreme El Niño events tend to be characterized by peak SST anomalies in the far eastern Pacific and are referred to as eastern Pacific (EP) El Niño, whereas a different type of event consists in peak SST anomalies confined to the central Pacific (CP). These events are referred as CP event (Kug *et al.*, 2009). Because the SST warming is located at a different place along the equator, these two types of El Niño events are associated with a distinct atmospheric teleconnection (Hastenrath, 1978; Ropelewski and Halpert, 1987; Barsugli and Sardeshmukh, 2002; Frauen *et al.*, 2014; Capotondi *et al.*, 2015). They are also associated with different oceanic teleconnections particularly in the absence of a persistent coastal warming off Peru during CP El Niño events, conversely to that during EP El Niño events (Dewitte *et al.*, 2012).

Recent studies have pointed out that the impact on rainfall along the coast of Peru is distinct during these two types of El Niño events (Lavado and Espinoza, 2014; Bourrel *et al.*, 2015; Rau *et al.*, 2017). EP El Niño events are associated with heavy rainfall in northern Peru while CP El Niño produces dryer conditions upstream along the Pacific slope. These studies focused on the average rainy season and on the peak phase of ENSO while events can differ in their evolution. Here we take a closer look at the relationship between ENSO and rainfall during strong El Niño events by observing that these events have different evolutions. Four strong El Niño events took place over the last five decades and produced noticeable rainfall in Peru: the 1972/1973, 1982/1983, 1997/1998 and 2015/2016 El Niño events. While not fully documented yet, we include in our analysis the recent 2015/2016 El Niño event as it has been recorded as the largest El Niño event to date since 1997. The selection of these events is based on the Niño3.4 index (i.e. SST anomalies averaged from 5°S to 5°N and 170° to 120°W). All these events had a comparable value of the Niño3.4 index at the peak phase of the event (1.9, 2.1, 2.3 and 2.3 °C, respectively, for December). While these events have comparable magnitudes, they present a different evolution and projection on SST anomalies in the tropical Pacific, which is thought to be influential on their teleconnections over Peru.

To illustrate the former statement, we present Figure 1 which shows the evolution of the so-called *C* and *E* indices defined by Takahashi *et al.* (2011) for these four events. The *E* and *C* indices are based on the first two PC time series of the empirical orthogonal function (EOF) analysis of SST over the tropical Pacific and account for the variability of the EP and CP El Niño events, respectively (see Section 2.3 for details). The composite evolution of the composite of the other 12 moderate El Niño events over the period 1950–2016 is also presented as a benchmark for comparison.

First, Figure 1 shows that the EP El Niño events are distinct from the CP El Niño events because the *E* index is characterized by large anomalies for EP El Niño, which is not the case for CP El Niño events. For the *C* index, the magnitude is comparable for both types of events although there is a tendency for lower values for EP El Niño than for CP El Niño events. The striking feature in Figure 1 is the large dispersion in the evolution of the *E* index for strong events with for instance, the 1997/1998 El Niño event peaking in December 1997, while the 1982/1983 presents a double peak, one in December 1982 and the other one in June 1983. The 1972/1973 El Niño peaked earlier in the year in August 1972 with still a secondary peak in December 1972, with also significantly lower values of the *E* index. The 2015/2016 El Niño event is more comparable to the 1972/1973 El Niño in terms of the magnitude of the *E* index, although it peaked in January 2016 while the 1972 El Niño peaked twice [in August (0) and December (0)]. Such dispersion in evolution and magnitude is likely to reflect onto precipitation along the coast, which is the focus of this article. In particular, we document the relationship between the temporal evolution of strong El Niño events and rainfall along the coast of Peru to gain knowledge in the local and large-scale factors that determine the extent and magnitude of rainfall. Our study can be viewed as an extension of former studies (Lavado and Espinoza, 2014; Bourrel *et al.*, 2015; Rau *et al.*, 2017) that focused on the impact of the two types of El Niño on rainfall. While these studies used the *E* and *C* indices to account for the ENSO variability at basin scale and investigate how rainfall in Peru projected onto these modes, our purpose is here to document the rainfall variability without assuming any *a priori* relationship with ENSO diversity. Our study is also motivated by the societal demand and the need to provide an interpretation of recent precipitation conditions in Peru associated with the 2015/2016 El Niño event that has been categorized as a strong event by the international community (L'Heureux *et al.*, 2017) while having much less dramatic consequences than the 1997/1998 El Niño for instance (SENAMHI, 2015). In that sense our study is also aimed at evaluating the nonlinearity of the ENSO teleconnection over Peru during strong El Niño event.

This article is structured as follows. Sections 2 and 3 provide a description of the study region, the *in situ* rainfall observed data set and El Niño indices, as well as the method for deriving the two main modes of variability in rainfall along the coast of Peru. Section 4 describes the characteristics of the modes and documents their statistical properties and relationship with ENSO. The four strong El Niño events are documented in the light of the obtained indices. Section 5 summarizes the results and discusses perspectives of this work.
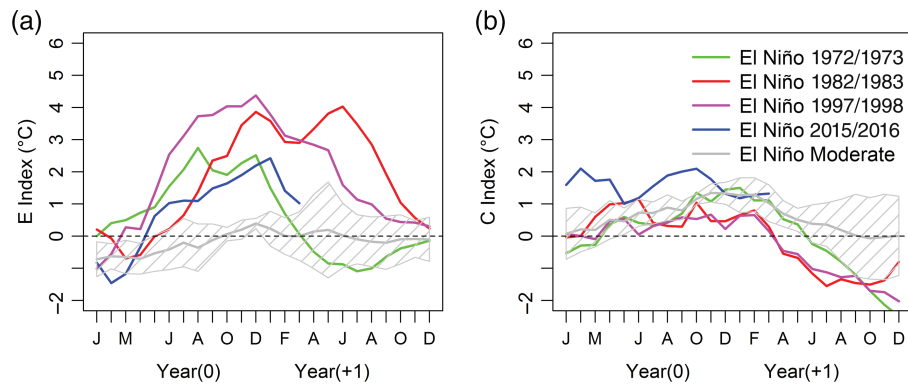
Figure 1. Evolution of the (a) E and (b) C indices of the four strong El Niño events (1972/1973, 1982/1983, 1997/1998 and 2015/2016) and the composite of moderate events. The E and C indices are defined as in Takahashi *et al.* (2011) from the HadISST data set over the period 1950–2016. The composite for moderate events includes 12 events from 1950 to 2016 (i.e. years 1957/1958, 1963/1964, 1965/1966, 1968/1969, 1969/1970, 1977/1978, 1987/1988, 1991/1992, 1994/1995, 2002/2003, 2004/2005 and 2009/2010). The hatching in grey line represents the dispersion (standard deviation) among the 12 moderate El Niño events. [Colour figure can be viewed at wileyonlinelibrary.com].

2. Study area and data sets

2.1. Study area

The Peruvian Pacific region is located from the shores of the eastern tropical Pacific to the west side of the Andes Mountains, between 3.5° and 18.5°S latitude and 69.5° and 80°W longitude (Figure 2). It presents an altitudinal west–east gradient that ranges from sea level to 4000 m above sea level (masl). It comprises a coastal strip as well as part of the Andes. The study area can be divided into an upper and lower region separated by an altitudinal level of around 1000 m (Brack and Mendiola, 2000; Rundel *et al.*, 2007). The lower region, that is, the coastal strip, is characterized by an arid climate with very low rainfall. The higher region exhibits a low mean annual rainfall of about 300 mm year^{-1}; average rainfall values increase with altitude and decrease with latitude progressing from northern to central areas. Large increases in rainfall are associated with the influence of oceanic warming in the EP during extreme El Niño events (Horel and Cornejo, 1986; Goldberg *et al.*, 1987; Tapley and Waylen, 1990; Bendix and Bendix, 2006; Douglas *et al.*, 2009; Cai *et al.*, 2014; Lavado and Espinoza, 2014; Bourrel *et al.*, 2015; Tedeschi *et al.*, 2015).

2.2. Monthly rainfall data set

The rainfall data set is composed of records from 145 meteorological stations distributed in lower and higher areas, ranging from sea level to 4406 m elevation, in the Peruvian Pacific region. These data were made available by the National Service of Meteorology and Hydrology of Peru (SENAMHI). The data set is composed of monthly rainfall data recorded over 52 years from 1964 to 2016 (see Figure 2 for the location of the stations). Missing data represent approximately 5% of the total data set. Quality control and homogenization of the data set were performed earlier by Bourrel *et al.* (2015) and Rau *et al.* (2017) using the regional vector method (taking into consideration elevation, watershed boundaries and latitude) and the significant correlation between the neighbouring stations.

A previous study on the north-central Peruvian Pacific (Bourrel *et al.*, 2015) presented a regionalization which defined nine regions (R1–R9) based on rainfall variability (see map of Figure 7). R1 and R3 correspond to the lower region located along the coast. R2 and R4–R9 represent highlands localized on the slopes of the Andes. Each climatically homogeneous region follows a rainfall regime based on proximal and homogeneous pluviometric stations and physiographic/topographic pattern constraints according to the regional vector methodology [RVM; Brunet-Moret (1979) cited by Bourrel *et al.* (2015)]. Rau *et al.* (2017) redefined these regions as a regionalized product along the whole Peruvian Pacific slope and coast following the RVM methodology combined with a *k*-means cluster analysis. This product showed the main modes of influence of the ENSO that influence the rainfall variability at seasonal and interannual time scales.

2.3. El Niño indices

In this study, we use the E and C indices as defined by Takahashi *et al.* (2011) based on SST data from the HadISST data set (Rayner *et al.*, 2003). These two indices are derived from the first two dominant principal components (PC) time series (PC1 and PC2) of the EOF analysis of SST over the tropical Pacific, as follows: $E = \frac{PC1 + PC2}{\sqrt{2}}$ and $C = \frac{PC1 - PC2}{\sqrt{2}}$.

They are independent by construction and depict the variability of EP El Niño (120°–90°E, 15°S–15°N) and CP El Niño events (170°E–100°W), respectively. These have been used in previous relevant studies to document ENSO teleconnections on rainfall in Peru (Lavado and Espinoza, 2014; Bourrel *et al.*, 2015; Rau *et al.*, 2017).

3. Methodology

3.1. Interpolation of rainfall

The quality-checked rainfall from the 145 meteorological stations was gridded at a spatial resolution of 0.5° using Cressman technique (Cressman, 1959; Doty, 1995). This
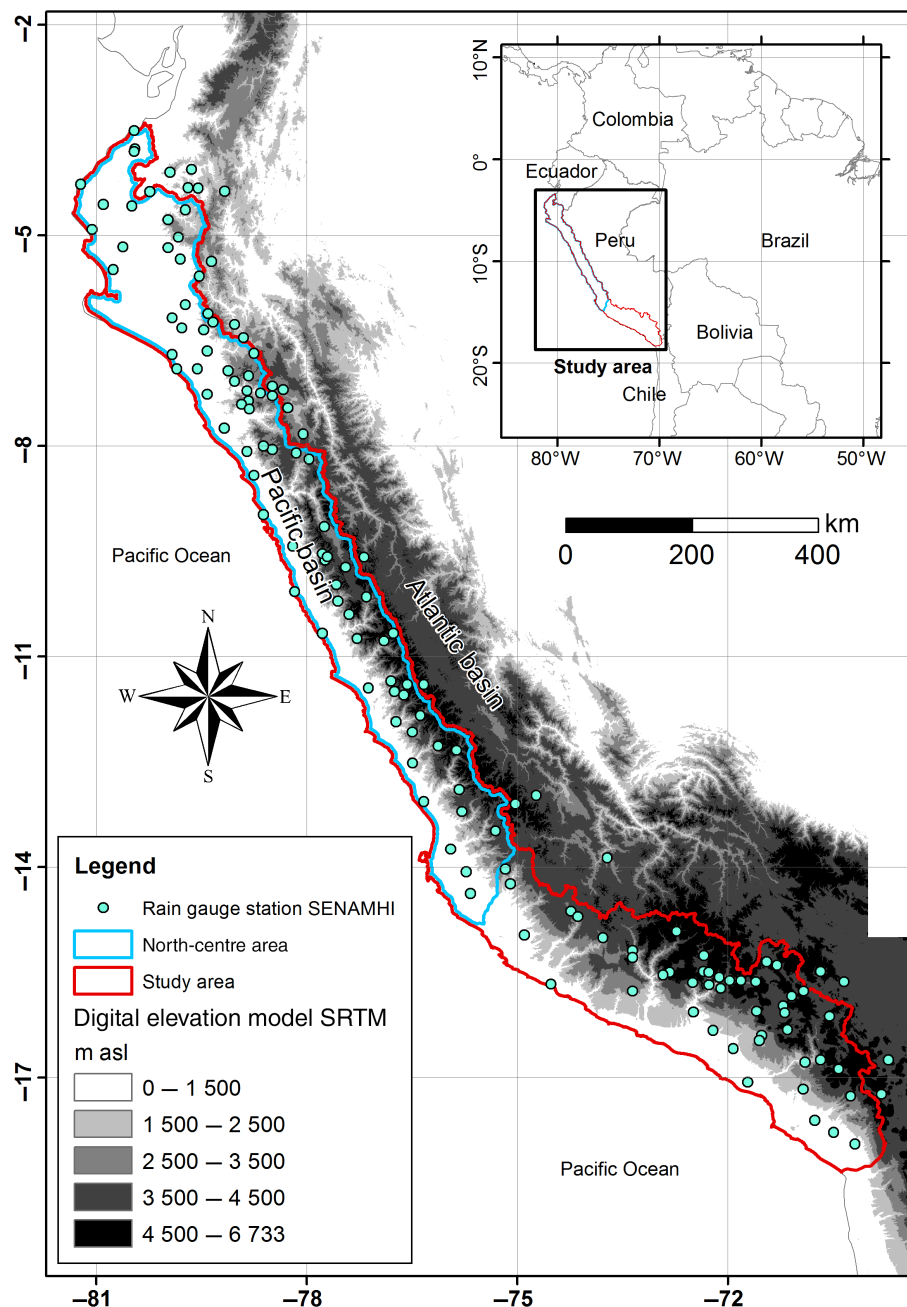
Figure 2. Map of the Peruvian Pacific slope (red outline) and north centre area (blue outline) (Bourrel *et al.*, 2015) and location of the 145 meteorological stations (turquoise dots) provided by the National Service of Meteorology and Hydrology of Peru (SENAMHI) from 1964 to 2016. [Colour figure can be viewed at wileyonlinelibrary.com].

spatial resolution was chosen as it represents the average distance between every station to its closest neighbours. The rainfall anomalies $(P - \overline{P})$, where P represents the observed monthly rainfall and $\overline{P}$ the mean climatology of rainfall, were computed over two distinct periods (1964–1977 and 1978–2016) to take into account the climate shift in the Pacific Ocean of the 1970s (Trenberth and Stepaniak, 2001), so that anomalies are referred to the mean seasonal cycle calculated over two different periods for the periods after and before 1977. Note that it was verified that has little impact on the results but still allows emphasizing anomalous events prior to 1977.

3.2.   EOF analysis of the rainfall data set

In order to characterize the rainfall variability, we use the EOF analysis. EOF modes are statistical modes that are aimed to grasp aspects of the physical mechanisms. However, sometimes some modes arise to satisfy the orthogonality conditions and do not necessarily have a simple physical interpretation. It is sometimes convenient to linearly combine EOF modes, which is equivalent to rotate the EOF modes, to infer mode patterns and associated time series that correspond readily to an observed process. The rotation is aimed at maximizing the variance along preferred directions that correspond to peculiar evolutions of

some events. In the case of our data set a strong positive skewness of the distribution is observed which corresponds to the impact of extreme ENSO events. It is therefore convenient to describe the variability along the direction of the evolution of extreme events from the first rotated mode. The second rotated mode more arises from the orthogonality condition and therefore accounts for the rainfall variability associated with moderate events. The angle of the rotation can be determined objectively from an EOF analysis in the space of the PC time series of the previous EOF analysis of the data.

Here, for precipitation data, the maximization procedure yields a rotation of 60° to be performed on the original EOF modes (PC1 and PC2). The corresponding indices are thus defined as follows: $Ep = \frac{PC1 - \sqrt{3}.PC2}{2}$ and $Cp = \frac{\sqrt{3}.PC1 + PC2}{2}$. The corresponding patterns are obtained by projecting the data onto these two indices through bilinear regression analysis. Regression analysis as a function of calendar month is also used to relate the Ep and Cp indices to the E and C indices, noting that they have a distinct seasonal evolution and seasonal phase locking. The significance of the regression coefficients was estimated using a t-test and retaining the 95% confidence level. At last, we also calculated composite evolution of precipitation anomalies based on the results of the EOF analysis that is averaging the associated time series of the rotated modes for extreme ENSO events over the time period covering the temporal evolution of the events (i.e. over 2 years). While the significance level is difficult to estimate for strong El Niño events (because they are too few), it was estimated for the composite of moderate El Niño events based on a bootstrap method (Efron and Tibshirani, 1993). The latter consisted in randomly selecting 7 events among the 12 events and calculate the composite. The operation is repeated 1000 times which allows estimating the PDF of the mean Cp and Ep values as a function of calendar month, yielding the threshold for the 95% significance level. These moderate 12 events were selected from Yu and Kim (2013).

4. Results

4.1. Modes of rainfall variability

As a first step, the rainfall variability is described based on the estimate of the two rotated EOF modes (Section 3.2). Figure 3(a) presents the phase space of the rotated EOF time series while Figure 3(b) displays the mode patterns. By construction the rainfall during extreme El Niño events should be accounted for by the Ep mode [x-axis of Figure 3(a)]. However, the striking feature of Figure 3(a) is that only the 1997/1998 and 1982/1983 El Niño events align along the x-axis during their developing phase (with little component on the y-axis), while the 1972/1973 and 2015/2016 El Niño events have their variance dominantly explained by the Cp mode (main projection along the y-axis). The 1972/1973 and 2015/2016 El Niño events

exhibit weak or moderate rainfall anomalies along the Cp mode, while the 1997/1998 and 1982/1983 El Niño events exhibit significant anomalous rainfall conditions along the Ep mode for at least 3 months (January–March).

The mode patterns (Figure 3(b)) reveal that the Ep mode that explains 34% of the explained variance has a strong loading in the northern Peru (Piura region) and consists in a meridional see-saw with a node at the latitude of ∼12°S (Lima). To the south of this critical latitude, rainfall anomalies during extreme El Niño events tend to be negative in the highland but still positive near the coast. The second mode pattern (Cp) explains 21% of the variance in rainfall anomalies and is characterized by a zonal east–west gradient that is more pronounced south of 15°S. This mode has its stronger loading in the inner domain indicating it is more related to high-altitude rainfall variability. The PC time series of the Ep (Cp) mode is correlated to the E (C) index at 44% (21%), which is significant at the 95% level. These relatively low values of correlation are likely associated with the distinct seasonality of rainfall and SST anomalies in the tropical Pacific during ENSO. This is investigated further in the subsequent section.

4.2. Seasonality and link with ENSO

While El Niño events tend to peak in austral summer [September (Y0) to January (Y1)], the rainy season in northern Peru concentrates around February (Y1) to April (Y1) (Bourrel *et al.*, 2015). There is thus a strong seasonal phase locking of the relationship between rainfall anomalies and ENSO. The seasonality of the relationship between ENSO and rainfall anomalies is investigated based on the rainfall and ENSO indices described previously. Figure 4 indicates that the peak variance for the Ep mode takes place in March while the Cp mode peaks in February. We note a sharp increase in rainfall variability from December to January for the Ep mode, which corresponds to the onset of the rainy season. The variance of the Cp mode also reduces earlier than that of the Ep mode suggesting more oceanic influence for the Ep mode, particularly associated with oceanic Kelvin wave activity (Bourrel *et al.*, 2015). By construction the Ep mode is positively skewed (skewness of Ep = 6.18) and thus relates the most to the E mode while the Cp mode is much more symmetric (skewness of Cp = 0.87). A bilinear regression analysis of the Ep and Cp modes onto the E and C indices provides the approximate Ep and Cp indices explained by E and C: Ep = 0.44*E + 0.04*C and Cp = 0.15*E − 0.24*C, which indicates that the Ep mode is mostly related to the E mode, while the Cp mode is influenced by both the E and C modes. Note the negative coefficient over C for Cp meaning that during a CP El Niño event (i.e. $C > 0$), Cp is negative so that the highlands along the coast experience a deficit of precipitation (Figure 3(b), right). In order to refine this analysis and take into account the marked seasonality in both the ENSO and rainfall indices (Figure 4), the climatological regression coefficients of the Ep and Cp indices onto the E and C indices are estimated, which consists in carrying the aforementioned regression analysis for each calendar month (Figure 5). The results of
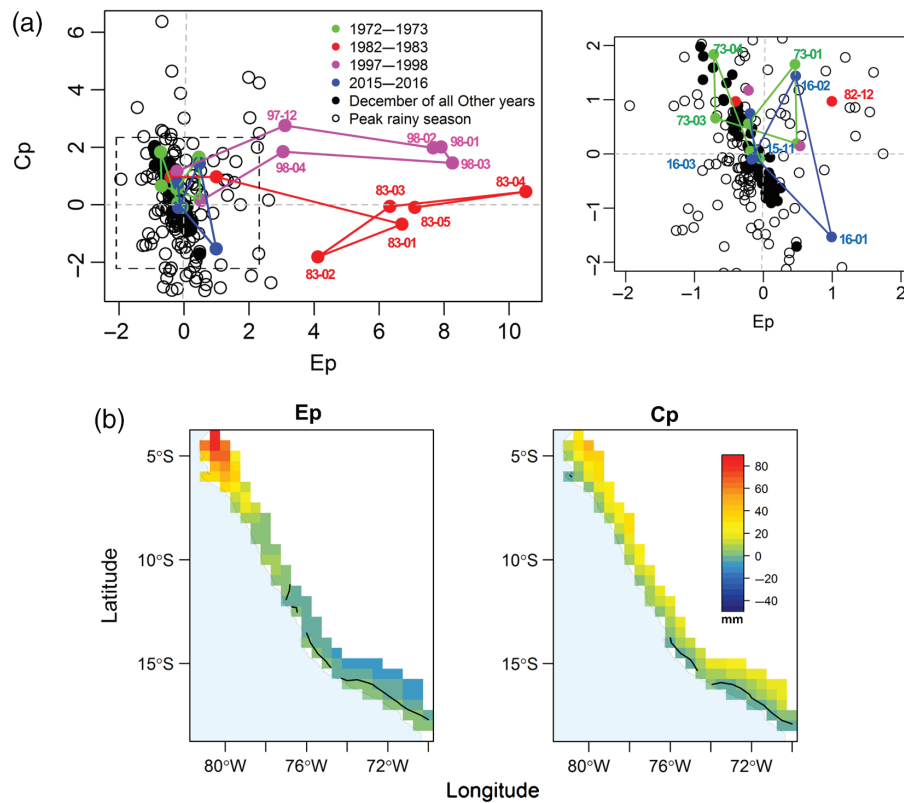
Figure 3. (a) Phase space of the evolution of the Ep and Cp modes. The evolution of the four strong El Niño event is highlighted with lines connecting the dots for the months between January of the first year J(Y0) and December of the second year D(Y1). (Y0: developing El Niño, Y1: decaying El Niño). The dots in black line correspond to the December value (Y1) of all other El Niño events. Zoom: (a) in interval [−2,2] (right-hand side). (b) Associated patterns (Ep and Cp) of rainfall anomalies over the period 1964–2016. Ep mode (first mode) (left-hand side) and Cp mode (second mode) (right-hand side). The thick black line indicates the zero contour. [Colour figure can be viewed at wileyonlinelibrary.com].

Figure 5 indicate that the Ep mode is tightly linked to the *E* index in March that is at the peak month of the rainy season. Interestingly, the Cp mode is also strongly related to the *C* index in February, which consists in an inverse relationship. Extreme El Niño events thus tend to yield a deficit in precipitation in the highland at the onset of the rainy season. Interestingly, the regression coefficient linking the Ep index to the *C* index peaks in April, which suggests that the magnitude of the SST anomalies in the CP (i.e. *C* mode) tends to determine the persistence of rainfall anomalies during extreme El Niño event in the northern region of Peru. On the other hand, strong EP El Niño event (*E* index) can also be influential on the Cp mode increasing precipitation in the highlands in April and December. In light of these results, in the following we take a closer look at the differences between the evolutions of the strong events.

4.3. Differences between strong events

Figure 6 shows the evolution of the Ep and Cp indices during the four strong El Niño events. The composite evolution of moderate El Niño events is also displayed so as to highlight the anomalous conditions during strong events. Clear differences in the evolution of the strong El Niño events can be observed. A striking feature revealed in Figure 6 is the large difference in the magnitude of the Ep

index at the peak of the events, with the 1997/1998 (Ep ≈ 8 in March) and 1982/1983 (Ep ≈ 6 in January and Ep ≈ 10 in April) being associated with a much larger rainfall anomaly in the northern part of Peru and an extended period of anomalous rainy conditions (lasting until June 1998 and July 1983) than the 1972/1973 and 2015/2016 El Niño events (Ep ≤ ±1). The 1972/1973 and 2015/2016 El Niño events also differ in terms of their projection on the Cp mode as the 1972/1973 event exhibits a positive value of the Cp index in January (Y1) while the 2015/2016 has a negative value of the Cp index, a situation that is inverted in the subsequent month [February (Y1)]. The evolution of the 1972/1973 and 2015/2016 El Niño events thus falls within the error for the composite of moderate El Niño events. Note also that the 1982/1983 and 2015/2016 El Niño events have a comparable negative value of the Cp mode at the peak phase, which is similar to the composite of the moderate El Niño events. This means that these two strong El Niño events were associated with a deficit in rainfall over the highlands. On the other hand, the 1997/1998 El Niño event also has a marked projection on the Cp but positive values during the rainy season, indicating that the highlands are associated with excess rainfall.

We now consider the regionalized product of Bourrel *et al.* (2015) in order to provide more details on the spatial variability of the impact of the strong El Niño events on
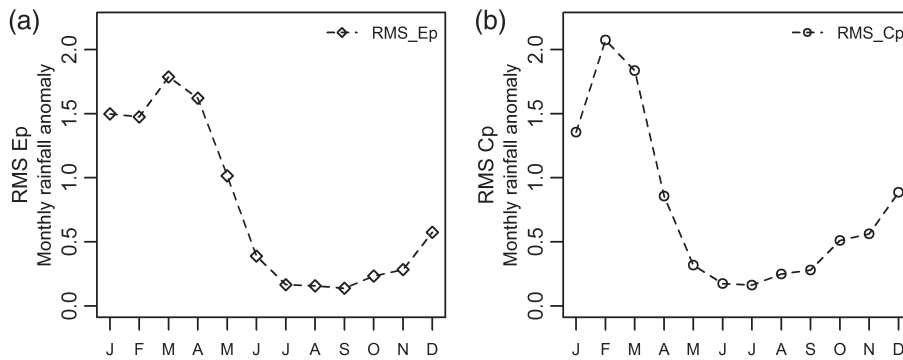
Figure 4. Climatological root mean square (RMS) of (a) the Ep mode and (b) Cp mode.
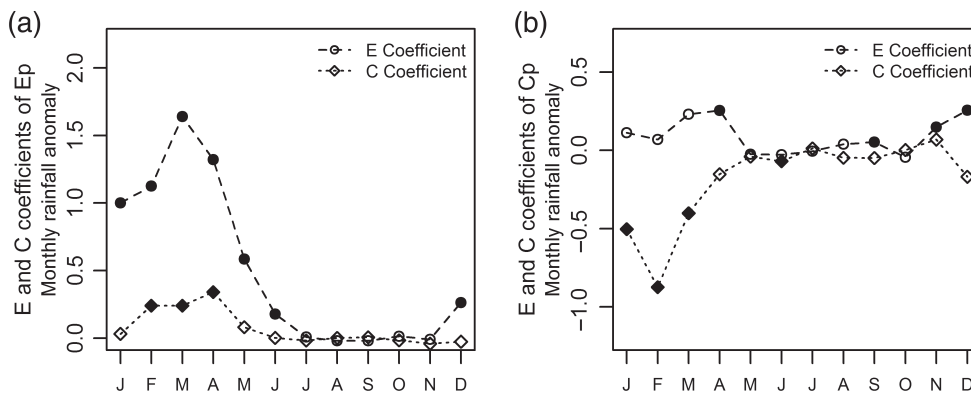

Figure 5. Climatological regression coefficients between (a) the Ep mode and the *E* and *C* indices (round), and the (b) Cp mode and the *E* and *C* indices (losange). The values of the coefficient that are statistically significant at the 0.05 level (*p*-value) are with filled symbol.

the precipitation responses. This is also considered a consistency check of the relevance of the Ep and Cp modes for depicting the rainfall anomalies associated with the strong El Niño events. Figure 7 provides the evolution of the Ep and Cp indices during the strong El Niño events along with the rainfall anomalies for the nine climatological homogeneous regions (Table 1) Bourrel *et al.* (2015). It indicates that the evolution of the Ep and Cp modes during the strong El Niño grasps in general the peculiarities of the homogeneous regions, with, in particular, the Ep mode accounting to a large extent for the rainfall anomalies in the R1, R2 and R3 regions during the 1997/1998 and 1982/1983 El Niño events, while the rainfall anomalies in the highland regions (R4–R9) evolving like the Cp mode for all events except during the 1982/1983 El Niño in R5–R7 and during the 2015/2016 El Niño. During the latter event, the Cp mode accounts for the evolution of rainfall anomalies only in the R1 region although the magnitude of the anomalies is underestimated by the Cp mode.

5. Discussion and conclusions

While El Niño events are generally classified from the amplitude of some indices at their peak phase (classically the NIÑO3.4 index), they can exhibit significant differences in their evolution, which is influential on their teleconnections and local impact. We have showed here that

the four strongest El Niño events of the last five decades are associated with a distinct rainfall anomaly evolution along the Pacific coast and slope. The different rainfall anomaly evolution during these El Niño events is interpreted as resulting from the contribution of two modes, the first mode accounting for heavy precipitation in the northern part of Peru and slight rainfalls in coastal zones southward, and characterized by a meridional see-saw pattern (Ep) with a node at the latitude of Lima (12°S), and the second mode associated with high variability (dryer and wet conditions) in the highlands along the coast and characterized by a marked zonal contrast (Cp). We show that the evolution of these two modes exhibits a large dispersion in evolution among strong El Niño events, with in particular the 1982/1983 and 1997/1998 El Niño events having the strongest impact by far over the northern region of Peru. The 1972/1973 and 2015/2016 El Niño events have a much weaker rainfall anomaly in the northern part of Peru and are statistically hardly distinguishable from the moderate El Niño events. The strong El Niño events are also in general associated with driest conditions over the highlands and to the South, with the 1982/1983 and 2015/2016 El Niño events exhibiting comparable negative anomalies of the Cp mode than the moderate El Niño composite. However, the 1997/1998 El Niño event was associated with significant positive rainfall anomalies over the highlands. The impact of the strong El Niño events over the highlands is thus also diverse.
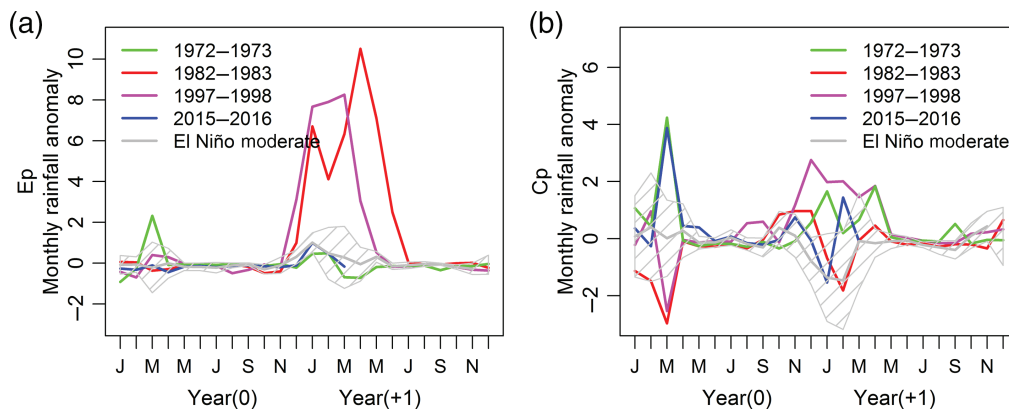
Figure 6. Evolution of the Ep and Cp modes during the four strong El Niño events and the composite of moderate events: Ep mode (left-hand side) and Cp mode (right-hand side). The composite for moderate events includes the same events than in Figure 1(b). The hatching in grey line represents the dispersion (standard deviation) among moderate El Niño events. [Colour figure can be viewed at wileyonlinelibrary.com].
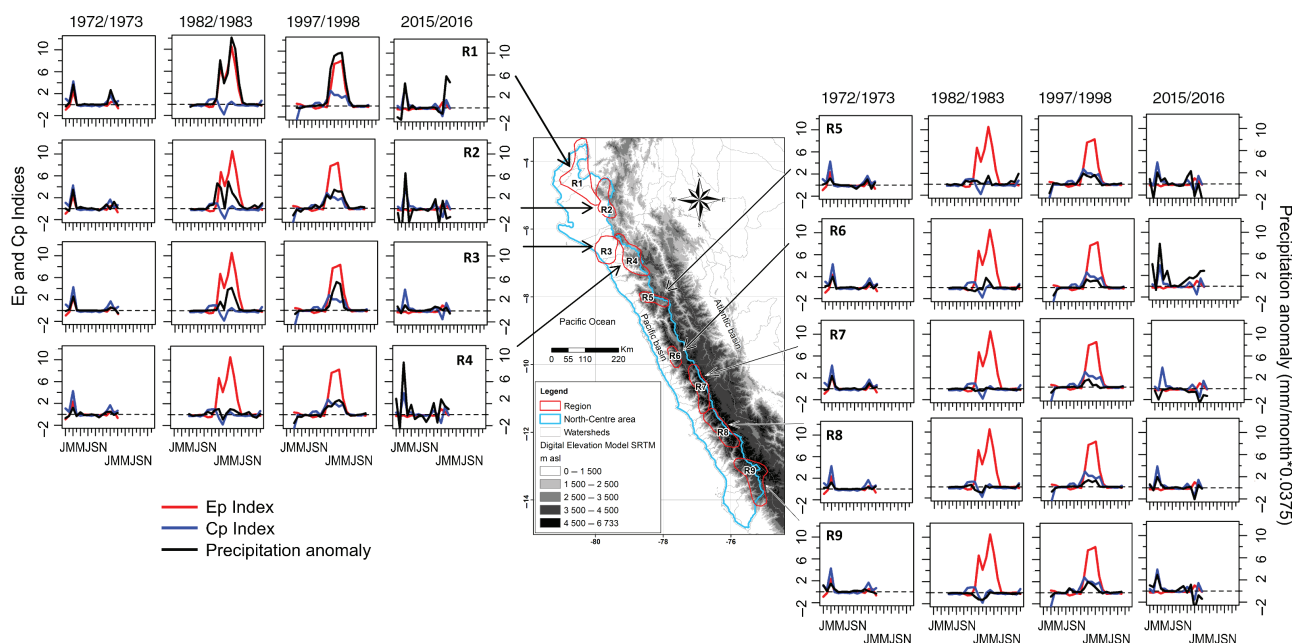

Figure 7. Evolution of the Ep and Cp indices and precipitation anomaly in the homogeneous regions during the four strong El Niño events 1972/1973, 1982/1983, 1997/1998 and 2015/2016. [Colour figure can be viewed at wileyonlinelibrary.com].

Overall, our results illustrate the nonlinear nature of the ENSO teleconnection of the rainfall over the western coast of Peru and the difficulty to predict anomalous rainfall conditions during strong El Niño events, which has a strong societal relevance. In particular, small changes in rainfall over highland areas can affect agriculture, water reservoir storage level and hydroelectric resources (BCRP, 2016). Our approach has been to model the complex of physical processes operating in nature with a linear statistical relationship between SST and rainfall variability during ENSO, which, although convenient for forecasting purpose, can be considered, oversimplified due to the diversity in forcing mechanisms of the anomalous rainfall in this region. Still our model takes into account the nonlinear evolution of ENSO through the consideration of the two ENSO regimes, which add a dimension to the commonly used approach. Among

the physical mechanisms producing heavy rainfall during strong EP Pacific El Niño events, the one associated with the deep convection triggered by SST when the latter is above ~26 °C (Woodman, 1999) can be used for the interpretation of the differences among events. The characteristics of SST along the coast of Peru during such events are likely influential on the distribution and magnitude of rainfall. As an illustration, we present Figure 8 that shows the evolution of the Niño1+2 index (based on total SST) during the four events. It shows that during the 1982/1983 and 1997/1998 El Niño events, the total temperature in the Niño1+2 region was above 26 °C for almost 6 months while during the 2015/2016 El Niño event, it only hardly reaches 26 °C during 1 month. The pattern of SST anomalies was also distinct between events (Figure 9), which could also drive mesoscale low-level atmospheric circulation and influence the distribution

Table 1. Observed monthly rainfall with respect to mean climatology (M. C. over the 1964–2016 period) during the El Niño events of 1972/1973, 1982/1983, 1997/1998 and 2015/2016 [between January of the developing year J(Y0) and December of the decaying year D(Y1)]. The dark green colour represents rain values above 80% of the monthly mean climatology. [Colour table can be viewed at wileyonlinelibrary.com].

		J	F	M	A	M	J	J	A	S	O	N	D	J	F	M	A	M	J	J	A	S	O	N	D
						Year (0)												Year (+1)							
	M. C.	46	78	125	58	21	5	1	0	0	1	2	12	46	78	125	58	21	5	1	0	0	1	2	12
R1	1972/1973	5	60	355	23	8	9	0	2	0	0	2	6	206	87	96	20	3	0	1	0	1	0	0	2
	1982/1983	2	2	0	16	1	0	0	0	0	1	5	90	597	372	509	893	707	266	26	0	3	2	0	12
	1997/1998	4	37	116	58	18	5	3	0	9	9	46	479	670	755	785	381	89	2	0	0	1	3	0	2
	2015/2016	18	59	259	78	43	3	1	0	0	3	4	3	35	271	263	–	–	–	–	–	–	–	–	–
	M. C.	118	194	257	152	40	15	4	6	13	29	31	65	118	194	257	152	49	15	4	6	13	29	31	65
R2	1972/1973	109	140	476	150	70	27	4	12	8	8	39	105	101	251	251	239	72	25	7	10	26	8	18	69
	1982/1983	90	115	39	118	48	2	2	0	5	65	80	387	380	223	601	348	182	58	16	0	23	69	44	143
	1997/1998	72	117	185	142	10	9	1	0	51	37	75	237	243	446	473	358	134	10	0	7	27	40	35	42
	2015/2016	108	95	444	90	47	4	2	0	0	31	78	4	168	172	229	–	–	–	–	–	–	–	–	–
	M. C.	14	25	54	15	4	1	0	1	1	3	3	3	14	25	54	15	4	1	0	1	1	3	3	3
R3	1972/1973	2	28	224	10	0	1	0	0	1	1	1	4	47	37	20	17	1	1	0	1	5	0	1	0
	1982/1983	1	4	1	7	0	0	0	0	1	4	7	16	126	52	308	297	155	19	0	0	1	9	0	1
	1997/1998	0	13	8	16	1	1	0	1	1	1	8	55	240	376	371	57	9	1	0	0	2	2	0	3
	2015/2016	38	23	81	27	9	1	0	1	5	11	24	20	20	49	40	–	–	–	–	–	–	–	–	–
	M. C.	103	131	171	106	48	22	14	17	44	80	61	68	103	131	171	106	48	22	14	17	44	80	61	68
R4	1972/1973	62	90	242	71	68	11	4	21	36	40	55	82	140	104	178	202	46	42	22	37	71	72	46	71
	1982/1983	62	74	57	87	59	6	6	4	43	115	78	136	164	92	196	184	107	51	13	22	73	59	28	87
	1997/1998	42	159	76	90	25	24	0	4	38	53	123	183	197	309	360	255	72	12	3	8	44	97	36	60
	2015/2016	173	83	435	111	99	1	5	5	6	75	122	41	170	192	209	–	–	–	–	–	–	–	–	–
	M. C.	114	136	168	93	30	12	7	10	28	67	49	74	114	136	168	93	30	12	7	10	28	67	49	74
R5	1972/1973	115	143	256	102	36	11	6	11	11	27	40	74	182	75	203	204	61	23	21	8	68	93	82	86
	1982/1983	61	55	90	105	28	0	7	3	13	104	80	125	156	159	165	200	16	17	0	2	23	102	78	212
	1997/1998	41	182	49	107	36	6	1	3	28	59	109	213	215	235	275	144	13	7	0	8	25	72	37	60
	2015/2016	139	82	217	111	54	6	7	0	15	55	87	144	56	153	88	–	–	–	–	–	–	–	–	–
	M. C.	68	92	122	43	8	1	1	2	6	27	29	41	68	92	122	43	8	1	1	2	6	27	29	41
R6	1972/1973	83	107	255	20	7	1	3	6	6	6	17	38	127	74	153	70	19	0	6	6	18	26	29	76
	1982/1983	26	54	53	29	2	0	0	1	0	4	5	4	57	78	241	112	0	0	0	0	4	8	17	18
	1997/1998	51	104	26	25	7	0	0	0	7	19	57	148	142	183	206	61	9	4	0	0	6	36	9	40
	2015/2016	177	81	333	82	83	0	3	0	19	56	79	87	118	175	199	–	–	–	–	–	–	–	–	–
	M. C.	91	106	118	40	9	2	1	3	10	30	33	61	91	106	118	40	9	2	1	3	10	30	33	61
R7	1972/1973	71	100	286	63	0	1	5	5	21	22	24	57	152	113	148	85	21	0	3	5	30	44	41	100
	1982/1983	94	114	52	24	0	0	1	0	1	43	42	37	77	81	120	44	2	6	0	0	2	13	24	57
	1997/1998	67	115	39	22	2	0	0	1	12	18	51	140	189	128	135	31	3	1	0	0	6	36	19	42
	2015/2016	84	52	102	39	10	1	0	3	1	12	22	48	24	73	72	–	–	–	–	–	–	–	–	–
	M. C.	76	91	99	29	5	1	1	2	5	15	18	50	76	91	99	29	5	1	1	2	5	15	18	50
R8	1972/1973	89	101	179	33	2	0	1	0	6	16	11	49	99	83	130	49	11	0	0	3	15	17	9	84
	1982/1983	58	92	56	18	2	1	2	1	4	29	47	19	20	26	115	19	6	2	1	2	2	3	13	80
	1997/1998	69	113	39	12	1	0	0	1	7	11	37	111	158	152	176	32	0	0	0	1	2	6	5	40
	2015/2016	94	84	152	48	2	1	0	4	2	10	24	58	22	109	96	–	–	–	–	–	–	–	–	–
	M. C.	97	112	118	37	8	3	2	5	9	16	20	50	97	112	118	37	8	3	2	5	9	16	20	50
R9	1972/1973	178	115	226	68	5	0	1	1	21	26	23	76	105	101	106	61	5	1	0	5	13	11	26	54
	1982/1983	73	117	64	6	1	0	0	0	0	13	13	2	13	28	51	41	3	0	0	0	0	0	13	45
	1997/1998	100	95	61	33	9	0	0	59	23	27	30	107	225	217	174	53	0	15	0	7	15	31	51	59
	2015/2016	122	134	186	49	7	4	1	5	20	42	16	83	3	95	71	–	–	–	–	–	–	–	–	–

of deep convection. The mechanisms associated with SST changes along the coast of Peru during El Niño events are tightly linked to both the El Niño equatorial dynamics (remote forcing) and upwelling dynamics (local forcing), which could thus be sources of the differences in rainfall between events. A recent study (Paek *et al.*, 2017) indicates for instance that the 2015/2016 El Niño event dynamics can be interpreted as resulting from processes associated with both the EP and CP El Niño events, conversely to the 1997/1998 El Niño that is diagnosed as a 'pure' EP El Niño event.

Other factors explaining the differences between events include the distinct characteristics between El Niño events of processes associated with synoptic variability due to either the Madden–Julian oscillation (Madden and Julian, 1972) or the extra-tropical storm activity of
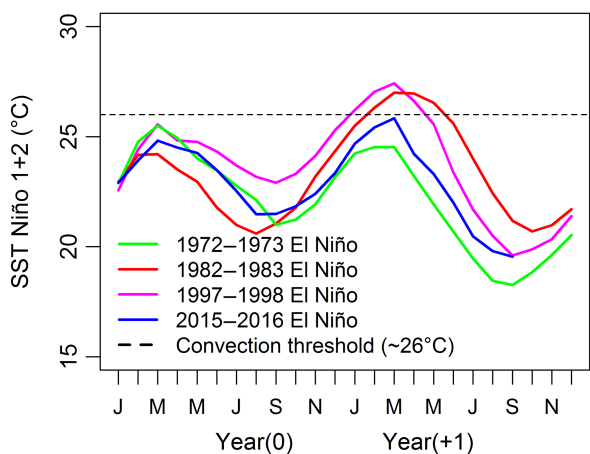
Figure 8. Evolution of the SST in the Niño1+2 region during the fourth strong El Niño events. The horizontal line indicates the convection threshold temperature (~26 °C). SST is obtained from the HadISST data set over the period 1950–2016. [Colour figure can be viewed at wileyonlinelibrary.com].

influencing the rainfall conditions during strong El Niño events (Takahashi and Martinez, 2017), our study calls for investigating the sensitivity of the rainfall distribution and evolution to the regional oceanic conditions, which could be through the use of a regional atmospheric model. This is planned for future work.

Noteworthy, while extreme El Niño events are forecasted to increase in frequency in a warmer climate (Cai *et al.*, 2014), our study suggests that there might not be a straight-forward relationship with the rainfall events over Peru considering the dispersion between events documented here over the observational record. In addition, one aspect that is not currently well accounted for in global coupled models is the regional SST anomalies along the coast of Peru and Ecuador (Takahashi *et al.*, 2014), which calls for investigating regional physical processes explaining such a diverse response of rainfall under strong El Niño conditions. Considering the likely impact of decadal variability on the relationship between ENSO and rainfall in Peru (Bourrel *et al.*, 2015; Segura *et al.*, 2016), the investigation of such processes would have to consider the influence of decadal variability.

the mid-latitudes that are influential on the along-shore winds along the coast of Peru (Dewitte *et al.*, 2011) or the South Pacific meridional mode (Zhang *et al.*, 2014). Local processes of air–sea interactions are also thought to be at work during El Niño events in this region (B. Dewitte, 2017; personal communication). While local SST anomalies are not likely to be the only factor
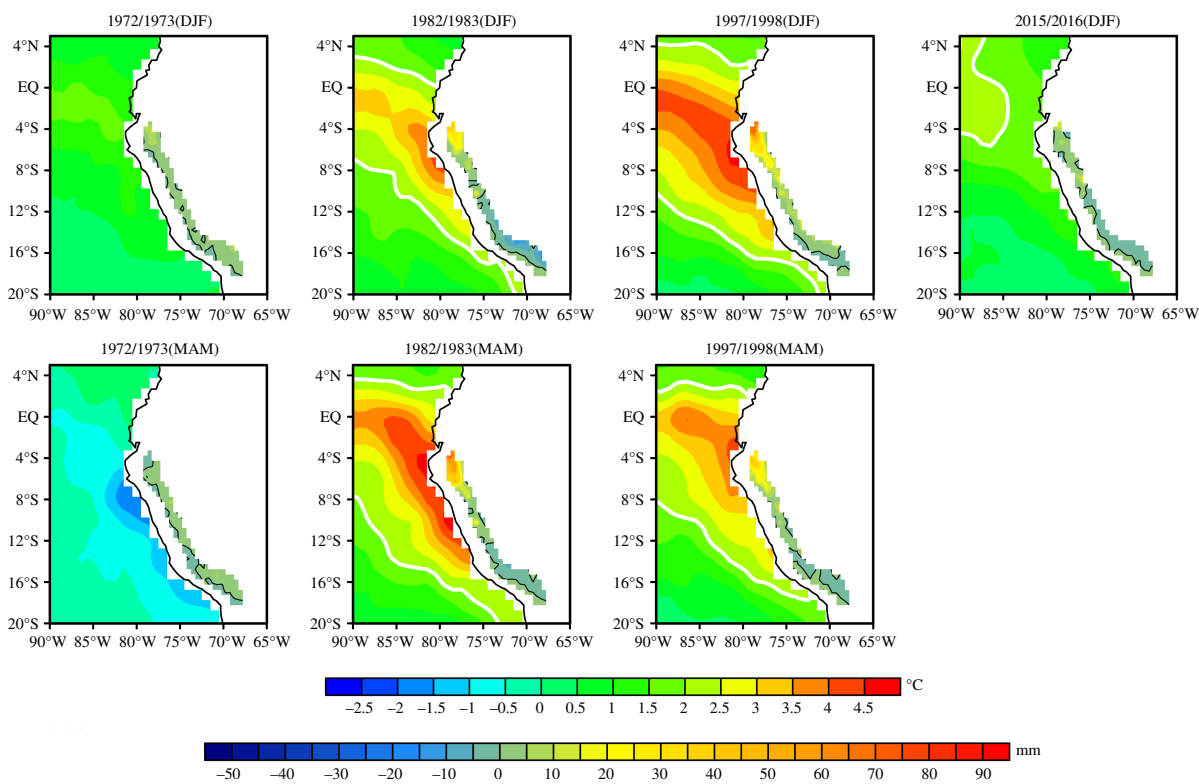
Acknowledgements

Figure 9. Evolution of SST and precipitation anomalies during the fourth strong El Niño events. Monthly averaged anomalies for (top) D(0)JF(+1) and (bottom) MAM(+1). Unit is in °C for SST (in the bottom right-hand corner) and in mm for precipitation (in the top right-hand corner for precipitation. For precipitation, the thick black line indicates the zero contour. For SST the contour in white line indicates the 2 °C isotherm. Anomalies are relative to the seasonal cycle calculated over the period 1964–1977 (1978–2008) for the 1972/1973 El Niño (the 1982/1983 and 1997/1998 El Niño). [Colour figure can be viewed at wileyonlinelibrary.com].

References

Barsugli JJ, Sardeshmukh PD. 2002. Global atmospheric sensitivity to tropical SST anomalies throughout the Indo-Pacific basin. *J. Clim.* **15**(23): 3427–3442.

BCRP. 2016. Actividad Económica (Marzo, abril y setiembre). Banco Central de Reserva del Perú (Central Reserve Bank of Peru). *Notas Estudio* **35**: 2–3 43: 2–3, 80: 2–4.

Bendix A, Bendix J. 2006. Heavy rainfall episodes in Ecuador during El Niño events and associated regional atmospheric circulation and SST patterns. *Adv. Geosci.* **6**: 43–49.

Bjerknes J. 1969. Atmospheric teleconnections from the equatorial Pacific. *Mon. Weather Rev.* **97**: 163–172.

Bourrel L, Rau P, Dewitte B, Labat D, Lavado W, Coutaud A, Vera A, Alvarado A, Ordoñez J. 2015. Low-frequency modulation and trend of the relationship between ENSO and precipitation along the northern to centre Peruvian Pacific coast. *Hydrol. Processes* **29**(6): 1252–1266.

Brack A, Mendiola C. 2000. *Ecología del Perú*. Editorial Bruño: Lima.

Brunet-Moret Y. 1979. Homogénéisation des précipitations. Cahiers ORSTOM. *Serie. Hydrol.* **16**: 3–4.

Cai W, Borlace S, Lengaigne M, van Rensch P, Collins M, Vecchi G, Timmermann A, Santoso A, McPhaden MJ, Wu L, England MH, Wang G, Guilyardi E, Jin F-F. 2014. Increasing frequency of extreme El Niño events due to greenhouse warming. *Nat. Clim. Change* **5**(2): 1–6. https://doi.org/10.1038/nclimate2100.

Capotondi A, Wittenberg AT, Newman M, Di Lorenzo E, Yu J-Y, Braconnot P, Cole J, Dewitte B, Giese B, Guilyardi E, Jin F-F, Karnauskas K, Kirtman B, Lee T, Schneider N, Xue Y, Yeh S-W. 2015. Understanding ENSO diversity. *Bull. Am. Meteorol. Soc.* **96**(June): 921–938.

Clarke AJ. 1983. The reflection of equatorial waves from oceanic boundaries. *J. Phys. Oceanogr.* **13**(7): 1193–1207.

Cressman GP. 1959. An operational objective analysis system. *Mon. Weather Rev.* **81**: 367–374.

Dewitte B, Illig S, Renault L, Goubanova K, Takahash K, Gushchina D, Mosquera K, Purca S. 2011. Modes of covariability between sea surface temperature and wind stress intraseasonal anomalies along the coast of Peru from satellite observations (2000-2008). *J. Geophys. Res.* **116**: C04028. https://doi.org/10.1029/2010JC006495.

Dewitte B, Vazquez-Cuervo J, Goubanova K, Illig S, Takahashi K, Cambon G, Purca S, Correa D, Gutierrez D, Sifeddine A, Ortlieb L. 2012. Change in El Niño flavours over 1958–2008: implications for the long-term trend of the upwelling off Peru. *Deep Sea Res. II: Trop. Stud. Oceanogr.* **77–80**: 143–156.

Diaz HF, Hoerling MP, Eischeid JK. 2001. ENSO variability, teleconnections and climate change climate variability; El Niño-Southern Oscillation (ENSO); teleconnections. *Int. J. Climatol.* **21**(15): 1845–1862.

Doty B. 1995. *The Grid Analysis and Display System-GrADS*. Center for Ocean-Land-Atmosphere Studies: Calverton, MD, 148 pp.

Douglas MW, Mejia J, Ordinola N, Boustead J. 2009. Synoptic variability of rainfall and cloudiness along the coasts of northern Peru and Ecuador during the 1997/98 El Niño event. *Mon. Weather Rev.* **137**: 116–136.

Efron B, Tibshirani RJ. 1993. *An Introduction to the Boot Strap*. Chapman and Hall: New York, 456 pp.

Frauen C, Dommenget D, Tyrrell N, Rezny M, Wales S. 2014. Analysis of the nonlinearity of El Niño-Southern Oscillation teleconnections. *J. Clim.* **27**(16): 6225–6244.

Goldberg RA, Tisnado GM, Scofield RA. 1987. Characteristics of extreme rainfall events in northwestern Peru during the 1982-1983 El Niño period. *J. Geophys. Res.* **92**(C13): 14225–14241.

Hastenrath S. 1978. On modes of tropical circulation and climate anomalies. *J. Atmos. Sci.* **35**: 222–223.

Horel JD, Cornejo GA. 1986. Convection along the coast of northern Peru during 1983: spatial and temporal variation of clouds and rainfall. *Mon. Weather Rev.* **114**: 2091–2105.

Horel JD, Wallace JM. 1981. Planetary-scale atmospheric phenomena associated with the Southern Oscillation. *Mon. Weather Rev.* **109**: 813–829.

Kao HY, Yu JY. 2009. Contrasting eastern Pacific and central Pacific types of ENSO. *J. Clim.* **22**(3): 615–632.

Keshavamurty RN. 1982. Response of the atmosphere to sea surface temperature anomalies over the equatorial Pacific and the teleconnections of the Southern Oscillation. *J. Atmos. Sci.* **39**: 1241–1259.

Kug JS, Jin FF, An SI. 2009. Two types of El Niño events: cold tongue El Niño and warm pool El Niño. *J. Clim.* **22**(6): 1499–1515.

Lavado W, Espinoza JC. 2014. Impactos de El Niño y La Niña en las lluvias del Perú (1965-2007). *Rev. Brasil. Meteorol.* **29**(2): 171–182.

L'Heureux ML, Takahashi K, Watkins AB, Barnston AG, Becker EJ, Di Liberto TE, Gamble F, Gottschalck J, Halpert MS, Huang B, Mosquera-Vásquez K, Wittenberg AT. 2017. Observing and predicting the 2015–16 El Niño. *Bull. Am. Meteorol. Soc.* **98**: 1363–1382. https://doi.org/10.1175/BAMS-D-16-0009.1.

Madden R, Julian P. 1972. Description of global-scale circulation cells in the tropics with a 40–50 day period. *J. Atmos. Sci.* **29**: 1109–1123.

Paek H, J-Y Y, Qian C. 2017. Why were the 2015/16 and 1997/98 extreme El Niños different? *Geophys. Res. Lett.* **44**: 1848–1856. https://doi.org/10.1002/2016GL071515.

Philander SGH. 1985. El Niño and La Niña. *J. Atmos. Sci.* **42**: 2652–2662.

Rau P, Bourrel L, Labat D, Melo P, Dewitte B, Frappart F, Lavado W, Felipe O. 2017. Regionalization of rainfall over the Peruvian Pacific slope and coast. *Int. J. Climatol.* **37**(1): 143–158.

Rayner NA, Parker DE, Horton EB, Folland CK, Alexander LV, Rowell DP, Kent EC, Kaplan A. 2003. Global analyses of sea surface temperature, sea ice, and night marine air temperature since the late nineteenth century. *J. Geophys. Res.* **108**(D14): 4407.

Ropelewski CF, Halpert MS. 1987. Global and regional scale precipitation patterns associated with El Niño/Southern Oscillation. *Mon. Weather Rev.* **115**: 1606–1626.

Rundel PW, Villagra PE, Dillon MO, Roig-Junent SA, Debandi G. 2007. Arid and semi-arid ecosystems. In *The Physical Geography of South America*, Veblen TT, Young K, Orme AE (eds). Oxford University Press: Oxford, UK, 158–183.

Segura H, Espinoza JC, Junquas C, Takahashi K. 2016. Evidencing decadal and interdecadal hydroclimatic variability over the Central Andes. *Environ. Res. Lett.* **11**(9): 1–8. https://doi.org/10.1088/1748-9326/11/9/094016.

SENAMHI. 2015. Escenarios de Peligros Hídricos en el Perú ante la ocurrencia de Eventos Niño Extraordinarios. Documento técnico elaborado por la Dirección General de Hidrología y Recursos Hídricos. Servicio Nacional de Meteorología e Hidrología del Perú, Lima, Peru.

Takahashi K, Martinez AG. 2017. The very strong El Niño in 1925 in the far-eastern Pacific. *Clim. Dyn.* https://doi.org/10.1007/s00382-017-3702-1.

Takahashi K, Montecinos A, Goubanova K, Dewitte B. 2011. ENSO regimes: reinterpreting the canonical and Modoki El Nino. *Geophys. Res. Lett.* **38**: L10704.

Takahashi K, Martínez R, Montecinos A, Dewitte B, Gutiérrez D, Rodriguez-Rubio E. 2014. Regional applications of observations in the eastern Pacific: Western South America. Whitepaper for TPOS2020, No. 8a, California, 1–31.

Tapley TD, Waylen PR. 1990. Spatial variability of annual precipitation and ENSO events in western Peru. *Hydrol. Sci. J.* **35**(4): 429–446.

Tedeschi RG, Grimm AM, Cavalcanti IFA. 2015. Influence of central and east ENSO on extreme events of precipitation in South America during austral spring and summer. *Int. J. Climatol.* **35**: 2045–2064.

Trenberth KE, Stepaniak DP. 2001. Indices of El Niño evolution. *J. Clim.* **14**: 1697–1701.

Trenberth KE, Branstator GW, Karoly D. 1998. Progress during TOGA in understanding and modeling global teleconnections associated with tropical sea surface temperatures. *J. Geophys. Res.* **103**(C7): 14291–14324.

Vargas P. 2009. El Cambio Climatico y sus Efectos en el Peru. Working Papers, World Bank, Washington, DC.

Woodman R. 1999. Modelo estadístico de pronóstico de las precipitaciones en la costa norte del Perú. El Fenómeno El Niño. Investigación para una prognosis, 1er encuentro de Universidades del Pacífico Sur: Memoria 93–108, Piura-Perú.

Yeh SW, Kug JS, Dewitte B, Kwon MH, Kirtman BP, Jin F-F. 2009. El Niño in a changing climate. *Nature* **461**(7263): 511–514.

Yu JY, Kim ST. 2013. Identifying the types of major El Niño events since 1870. *Int. J. Climatol.* **33**(8): 2105–2112.

Zhang H, Clement AC, DiNezio P. 2014. The South Pacific meridional mode: a mechanism for ENSO-like variability. *J. Clim.* **27**: 769–783. https://doi.org/10.1175/JCLI-D-13-00082.1.